Observation and Characterization of Dicarbonyls on a RhCu Single-Atom Alloy

Yicheng Wang[1], Julia Schumann*[2,3,4], Elizabeth. E. Happel[1], Volkan Cinar[1], E. Charles H. Sykes[1], Michail Stamatakis[2], Angelos Michaelides[3,4], Ryan T. Hannagan*[1]

[1] Department of Chemistry, Tufts University, Medford, Massachusetts 02155, USA

[2] Department of Chemical Engineering, University College London, London WC1E 7JE, UK

[3] Yusuf Hamied Department of Chemistry, University of Cambridge, Cambridge CB2 1EW, UK

[4] Department of Physics and Astronomy, University College London, London WC1E 6BT, UK

* Corresponding authors: r.t.hannagan@gmail.com & j.schumann@ucl.ac.uk

Abstract

Dicarbonyl species are ubiquitous on Rh/oxide catalysts and are known to form on Rh^+ centers. However, dicarbonyl species have never been directly observed on single-atom alloys (SAAs) where the active site is metallic. Herein, using surface science and theoretical modeling, we provide evidence of dicarbonyl species at isolated Rh sites on a RhCu(100) SAA. This approach not only enables us to directly visualize dicarbonyl species at Rh sites, but also demonstrate that the transition between the mono and dicarbonyl at Rh sites can be achieved by changing surface temperature and CO pressure. Density functional theory calculations further support the mono and dicarbonyl assignments and provide evidence that these species should be stable on other SAA combinations. Together, these results provide a picture of the structure and energetics of both the mono and dicarbonyl configurations on the RhCu(100) SAA surface and should aid with IR assignments on SAA nanoparticle catalysts.

TOC

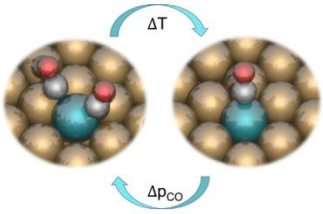

Keywords: Single-Atom Alloy, CO Infrared Spectroscopy, Surface Science, Density Functional Theory, Rhodium-Copper Bimetallic

CO infrared spectroscopy is a ubiquitous tool used in catalyst characterization due to the sensitivity of the C-O stretch frequency to different surfaces and binding sites.[1,2] This technique has been widely applied to study CO oxidation on supported metal nanoparticles, as well as used in the characterization of active sites in single-atom catalysts.[3–7] However, definitive peak assignments on complex catalysts samples is challenging. While the fast growing field of single-atom catalysis has produced many promising catalysts for a variety of reactions, definitively attributing catalytic activity to single atom or cluster sites can been difficult and controversies exist in the literature over the assignment of IR spectra.[3,6]

Single-atom alloys (SAAs) are a type of single-atom catalyst consisting of a somewhat inert host metal doped with single atoms of a more reactive metal.[8–16] Unlike most catalysts, single-atom alloys were discovered using fundamental microscopy and desorption measurements on single crystals under model-system Ultra-High Vacuum (UHV) conditions before making the transition to nanoparticle analogs. Since these initial studies, close synergy between model-system work under UHV and nanoparticle studies under industrially relevant conditions has enabled the design and understanding of these materials. Several nanoparticle catalysts have been developed using this combined methodology, and some examples include: RhCu SAAs for propane dehydrogenation,[9] PdCu SAAs for acetylene semi-hydrogenation to ethylene,[14] and NiAu SAAs for the dehydrogenation of ethanol.[11]

While dicarbonyl species have been observed on single-atom catalysts consisting of metal atoms supported on oxides, these species have not been reported on SAAs.[17,18] Furthermore, it would not be expected that dicarbonyls would be stable on SAAs considering that they normally form on Rh^+ species according to the 18 electron rule.[19–22] It is well known that atomically dispersed Rh atoms on oxide supports exhibit two characteristic CO IR peaks which correspond to the asymmetric and symmetric stretch of the dicarbonyl at isolated Rh sites.[19,23–27] In fact, the appearance of these spectral features (and the absence of linear and bridge bound CO, characteristic of CO adsorption on nanoparticles) is often considered as strong evidence of active site dispersion on oxides.[25,28]

Herein, we examine a well-defined RhCu(100) SAA surface to understand CO adsorption at the active site. Using a combination of temperature programmed desorption (TPD) and reflection absorption infrared spectroscopy (RAIRS), we find two unique features in the spectra: a weakly bound dicarbonyl feature at 1926 cm^{-1} (stable below ~265 K), and a strongly bound monocarbonyl feature at 1978 cm^{-1} (stable below ~440 K). Due to the surface selection rules on metallic samples, we only observe the symmetric feature, unlike dicarbonyls on metal oxides where both symmetric and asymmetric bands are observed. To confirm our assignments, we exposed the surface to an isotopic mixture of CO which led to the band associated with the symmetric dicarbonyl stretch splitting into three features, while the band associated with the monocarbonyl stretch split into two, consistent with the expected isotopic scrambling. Interestingly, we found that even modest pressures of CO (~1×10^{-6} mbar) can cause the conversion of the monocarbonyl feature to the dicarbonyl at room temperature. This is the first observation of dicarbonyls on SAAs and is important in terms of catalyst characterization, but may also have broader implications, since the dicarbonyl structure may act as a reaction intermediate for C-C coupling in CO_2 reduction.

Previous results have shown that low coverages of Rh in Cu exist as isolated sites forming a SAA.[17,29] This is in agreement with theoretical studies which show that the formation of small Rh ensembles (such as dimers and trimers) is endothermic in Cu.[30,31] Interestingly, due to the kinetics of alloy formation under model system conditions, we have previously found that the host metal

facet (111 vs 100) impacts the dispersion of the active sites.[17,29] On RhCu(100), single Rh atoms are finely dispersed across the entire surface, while on RhCu(111) most of the isolated Rh atoms are located in dense brims in the regions above the step edges. Density Functional Theory (DFT) calculations demonstrated that these observed Rh distribution differences between RhCu(100) and RhCu(111) were due to different alloying mechanisms on the two different surface facets.[29] Specifically, the diffusion barrier for Rh atoms on Cu(100) is higher than that on Cu(111) and therefore direct atomic exchange of Rh into the terraces is favored on Cu(100). This results in the observed well dispersed Rh atoms in Cu(100) while dense alloyed brims are formed in the regions above the step edges on Cu(111) due to the higher diffusion rate on Cu(111) that enabled the Rh atoms to reach step edges and place exchange into the surface at those sites.[29]

In order to further study the properties of isolated Rh sites in Cu(100), 0.7% of a monolayer of Rh was deposited on Cu(100) at 300 K, the surface was cooled, and CO TPD and IR spectroscopy were conducted. As shown by the TPD results in Fig. 1A, we observe the desorption of CO from the c(2×2) phase on Cu(100) <180 K.[32] These results are consistent with previous reports as well as our controls on Rh-free Cu(100) presented in Fig. 1A (black trace).[32,33] At higher temperatures, two features, which are found only in the presence of Rh, are observed at ~265 K and ~440 K. The high temperature feature at ~440 K corresponds to CO bound in a mono-dentate configuration to the isolated Rh atoms.[17] However, the feature at ~265 K has never been observed before. To rule out the possibility that defect sites such as steps and kinks on the Cu(100) surface could be responsible for this desorption feature, we intentionally increased the step edge density of the crystal via argon ion bombardment at 300 K.[34] This led to the appearance of an additional CO desorption feature at 200 K (grey trace),[32] indicating that the desorption peak at ~265 K is associated with the Rh atoms not Cu defect sites. The ratio of the area of the low temperature Rh feature to the high temperature feature is ~1:1 which is consistent with adsorption of two CO molecules at each Rh site in a dicarbonyl configuration.

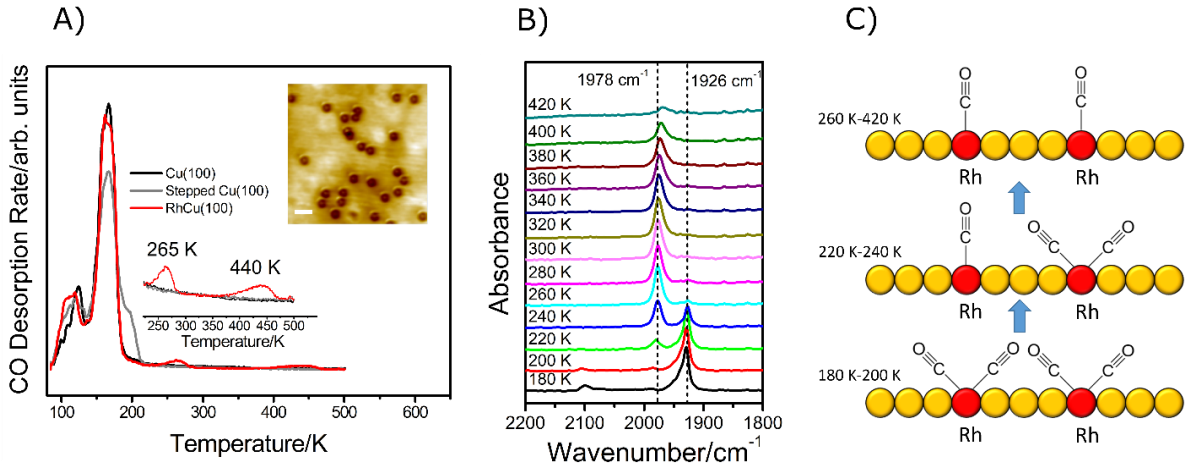

Fig. 1. TPD and RAIRS results showing two distinct binding sites for CO on isolated Rh atoms in Cu(100). A) TPD spectra of saturation CO exposures on Cu(100), roughened "stepped" Cu(100), and a 0.7% RhCu(100) SAA. A magnified view of the high temperature desorption features is shown above the TPD traces. The inset shows an STM image of a Rh/Cu(100) SAA in which the Rh sites appear as depressions. Image conditions: 300 mV, 300 pA, scale bar is 2 nm. B) RAIRS spectra of saturation CO on RhCu(100) SAA as a function of temperature. All spectra were obtained at the indicated temperatures. C) Schematic illustration of the proposed structure of the low and high temperature carbonyls.

To aid assignment of these features, we computed the stability of CO bound to Rh in the mono and dicarbonyl configurations using DFT as shown in Table S1. These results demonstrate the formation of a dicarbonyl at the Rh dopant atom is more stable (-2.90 eV, with the particular exchange-correlation functional used, see Supporting Information) compared to a situation where there is only one CO molecule adsorbed on Rh and the other CO is adsorbed on the Cu host (-2.40 eV). This result is initially very surprising, given there is usually a strong steric and electronic CO-CO repulsion on metal surfaces that prevents CO from aggregating at low and intermediate coverages.[35,36] However, dicarbonyl formation on SAAs can be rationalized by the strong adsorption energy of CO on the Rh dopant and the associated energy gain ΔE from moving the CO from the weakly binding Cu host to the dopant, that outweighs the steric and dipole repulsion upon bringing two CO molecules close together. The calculations show that the desorption energy of CO from the dicarbonyl configuration is lower (1.09 eV) than the monocarbonyl (1.81 eV), but still stronger than on the Cu host (0.59 eV), in agreement with the experimental values derived from Redhead analysis with a pre-factor of 10^{15} as obtained for the desorption of CO under the assumption of a late 2D gas-like transition state (0.8 eV for the peak at ~265 K and 1.4 eV for the peak at ~440 K, see Supporting Information).

In order to better understand the behavior of the carbonyls as a function of temperature and pressure, CO RAIRS experiments were conducted by exposing the as-prepared RhCu(100) SAA to a saturation coverage of CO at 180 K and collecting IR spectra at increasing surface temperature. As shown in Fig. 1B, two peaks at 2099 cm^{-1} and 1926 cm^{-1} were observed. The peak at 2099 cm^{-1} originates from CO on Cu and disappears by 220 K, consistent with our TPD data.[32] Upon further increasing the temperature such that CO is only bound to Rh sites, the feature at 1926 cm^{-1} shrinks and a peak at 1978 cm^{-1} appears. According to our theoretical modeling, the monocarbonyl and symmetric dicarbonyl stretches should appear at 1934 cm^{-1} and 1891 cm^{-1} with a 43 cm^{-1} interval. This 43 cm^{-1} difference is in good agreement with the 52 cm^{-1} interval in the experimental results (1978 cm^{-1} for monocarbonyl vs 1926 cm^{-1} for dicarbonyl).[17,30,37] The ~40 cm^{-1} offset between the experiment and theory is typical of similar studies.[37,38]

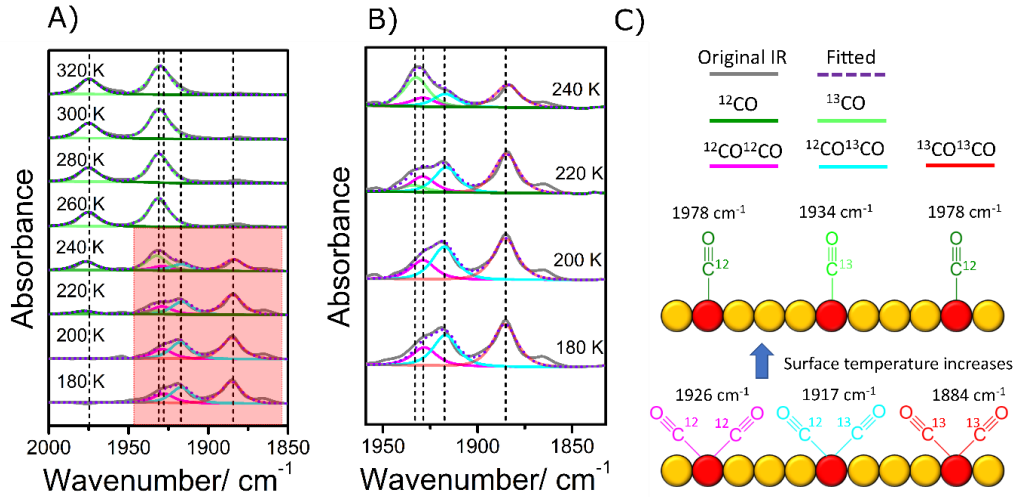

Fig. 2. Isotopic evidence of mono and dicarbonyl assignments. A) RAIRS spectra after exposing saturation coverage of a 2:3 ratio $^{13}C^{16}O$:$^{12}C^{16}O$ mixture to 0.7% RhCu(100) and taking the IR spectra over the temperature range 180 K to 320 K with peak fitting. B) Expanded view of red highlighted region in panel

A. C) Schematic illustration of the three isotopically labelled dicarbonyl species observed between 180 K and 320 K. All spectra were obtained at the indicated temperatures.

While dicarbonyls are typically identified by their characteristic symmetric and asymmetric stretches, due to the surface selection rules on metals, only the symmetric stretch is observed (see Fig. S2 for details).[39] In order to further support our mono and dicarbonyl assignments, we exposed the RhCu SAA surface to a mixture of $^{13}C^{16}O$ and $^{12}C^{16}O$ (the $^{13}C^{16}O$:$^{12}C^{16}O$ ratio was 2:3 as measured by mass spectroscopy). This is a well-known approach for the identification of dicarbonyl species when only symmetric modes can be observed.[39] Specifically for this case, the monocarbonyl should exhibit two peaks arising from the (^{13}CO)-Rh and (^{12}CO)-Rh stretches. In contrast, the dicarbonyl should exhibit three peaks due to the symmetric stretches of the (^{13}CO)-Rh-(^{13}CO), (^{13}CO)-Rh-(^{12}CO), and (^{12}CO)-Rh-(^{12}CO) dicarbonyls.

Consecutive IR spectra were then taken at 20 K intervals starting from 180 K. As shown in Fig. 2A, when the surface temperature is 180 K, three peaks (1926 cm^{-1}, 1917 cm^{-1} and 1884 cm^{-1}) are observed which correspond to (^{12}CO)-Rh-(^{12}CO), (^{12}CO)-Rh-(^{13}CO) and (^{13}CO)-Rh-(^{13}CO) symmetric stretching modes, respectively. The intensity of these initial features starts to diminish as the surface temperature increases. At 220 K, IR peaks at 1978 cm^{-1} and 1934 cm^{-1} are observed. These two peaks can be assigned to monocarbonyl species at isolated Rh sites (1978 cm^{-1} and 1934 cm^{-1} peaks corresponding to $^{12}C^{16}O$ and $^{13}C^{16}O$, respectively). This observation agrees with the IR data in Fig. 1B where dicarbonyl species begin to convert into monocarbonyl species at ~220 K. Importantly, in our TPD experiments, we observe a desorption maximum for half of the CO adsorbed at Rh sites at ~265 K, which is consistent with the temperature at which we observe the complete conversion of dicarbonyl features to monocarbonyls in the RAIRS measurements. This provides further support for our IR assignments of a lower temperature dicarbonyl state and a high temperature monocarbonyl species.

As we have described, the relative populations of the mono and dicarbonyls can be controlled by surface temperature, and we now discuss how these species are affected by CO pressure (Fig. 3). Exposure of the surface to saturation CO at 250 K followed by pumping down to UHV results in a mixture of dicarbonyl and monocarbonyl species as evidenced by the peaks at 1978 cm^{-1} and 1926 cm^{-1}. Heating to 300 K converts the dicarbonyl species at 1926 cm^{-1} to the monocarbonyl species at 1978 cm^{-1}. However, when we backfill the chamber and conduct the RAIRS experiments in-situ, we see a steady increase in the dicarbonyl configuration with increasing pressure. At 300 K and 1×10^{-6} mbar CO, nearly all of the Rh exists in the dicarbonyl configuration. Further evacuation of the CO leads to the disappearance of dicarbonyl peak and again the monocarbonyl species becomes dominant. The result indicates that we can reversibly transition between monocarbonyl and dicarbonyl species at the Rh sites by changing the CO partial pressure in the chamber.

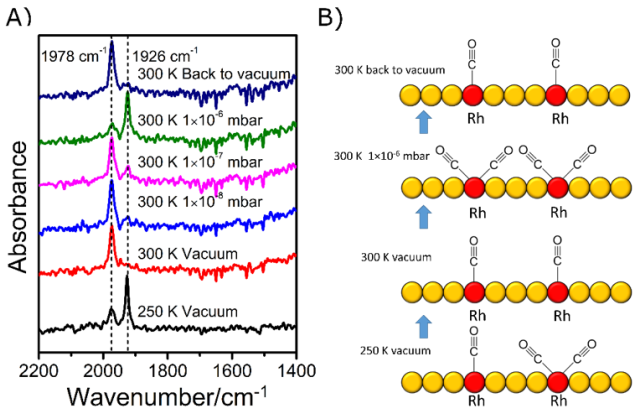

Fig. 3. In-situ RAIRS experiments showing pressure induced conversion of mono to dicarbonyl species. A) RAIRS spectra as a function of CO pressure on 0.7% RhCu(100) SAA. B) Schematic illustration of the process. All spectra were obtained at the indicated temperatures.

Using LT-STM, we are also able to directly visualize the dicarbonyl species observed in the TPD and IR experiments. As shown in Fig. 4, dicarbonyl species (red arrows) appear as dark linear three-lobed depressions while the CO-free Rh atoms appear as bright protrusions (green arrows). These dicarbonyl features are similar in appearance to those previously observed via STM for Fe atoms deposited on top of a Ag(110) surface, in which the dicarbonyl appears as a linear depression feature.[40] It is important to note that the dicarbonyl species we observe in Fig. 4A aligned with both high symmetry directions of the Cu(100) lattice, which enabled us to rule out the possibility that their shape was an artifact of the STM tip. By conducting localized STM tip pulses on each of the dicarbonyl features,[41] we were able to remove the adsorbed CO and reveal the Rh atoms underneath the dicarbonyl features as shown in panel b. It can be seen that there is a Rh atom at the center of where each dicarbonyl feature had been observed, thereby confirming the adsorption site of the dicarbonyls as a single Rh atom site.

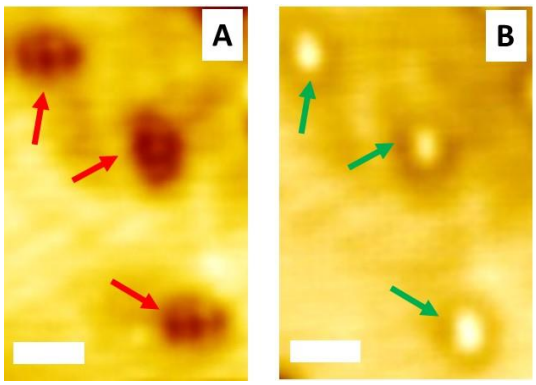

Fig. 4. 5 K STM images after CO adsorption on RhCu(100) SAA. A) STM image after adsorption of CO followed by ~220 K anneal to populate Rh sites but not Cu. Red arrows highlight three dicarbonyl features, two oriented horizontally and one vertically. B) STM image of the same area after -3 V STM tip pulses were used to remove the CO from the Rh sites. Green arrows correspond to the CO-free Rh atom sites on which the dicarbonyl species were adsorbed. Imaging conditions in both cases: 12 mV, 500 pA. The scale bar is 1 nm in both images.

Based on this unexpected observation of the dicarbonyl species on a metallic Rh center, we assessed the possibility of dicarbonyl formation on other SAA surfaces with late transition metal dopants. Fig. 5A shows the spillover energies (ΔE) of dicarbonyls on 5 different SAAs in both the 100 and 111 facet of Cu. This ΔE correspond to the energy necessary to move the 2nd CO from the host metal to a dopant bound to a single CO. Negative values of ΔE in this case mean a favorable dicarbonyl formation. It can be seen that, (i) RhCu(100) has the highest preference for the formation of the dicarbonyl species; (ii) the more open (100) surface has a higher stability of the dicarbonyl species than the close-packed (111) surface; and (iii) the stability trends of the dicarbonyl do not follow the stability of the monocarbonyl adsorbates as compared with literature values.[30,31] For example, the IrCu(111) SAA binds one CO in a monocarbonyl configuration stronger than RhCu(111), however, RhCu(111) binds the second CO in a dicarbonyl configuration stronger than IrCu(111). Importantly, these results indicate that other SAAs, beyond what was studied experimentally in this paper, should form dicarbonyls.

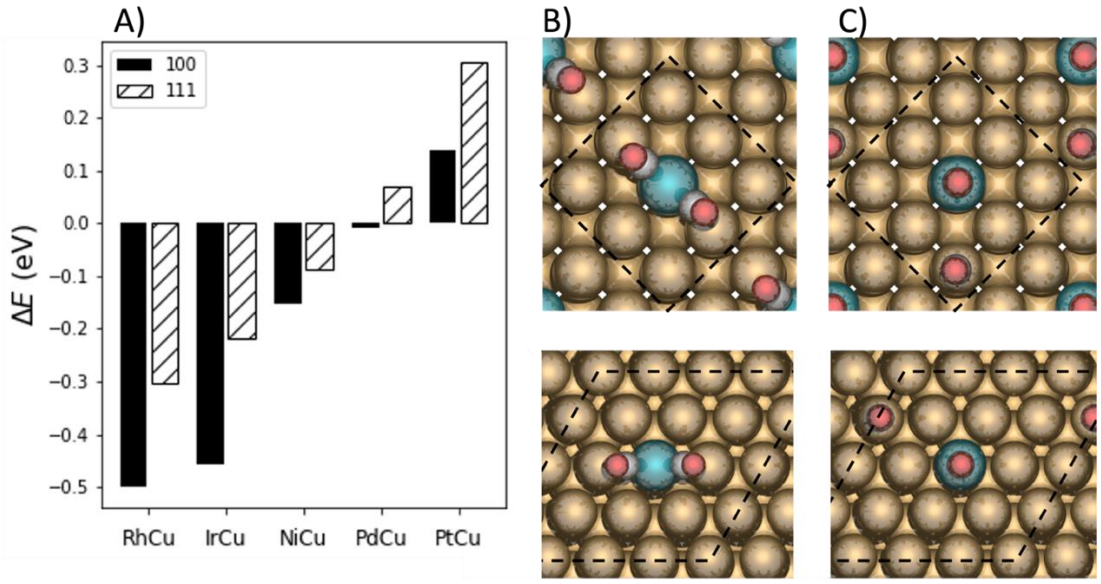

Fig. 5. DFT calculated stability of the dicarbonyl adsorbate configuration relative to separated monocarbonyl species on dopant and host. A) Dicarbonyl spillover energies of 5 different SAAs with different surface terminations: (100) and (111). B) Structure of the dicarbonyl adsorbate on RhCu(100) (top) and RhCu(111) (bottom). C) Structure of the separated monocarbonyl species on dopant and Cu host surfaces. Carbon atoms are colored in grey, oxygen atoms in red, Rh atoms in blue, and Cu atoms in brown.

Using a combination of CO TPD, RAIRS, and STM we were able to characterize and directly visualize the binding of CO to isolated Rh atoms in the surface of Cu(100). We find that Rh atoms in these SAAs are able to coordinate two CO molecules in a dicarbonyl configuration at low temperature (<260 K) under UHV conditions, in agreement with theoretical modelling. However, at room temperature the dicarbonyl state can also be populated with modest standing pressures of CO (~1×10^{-6} mbar). Importantly, due to the surface selection rules of adsorbate vibrations on metal surfaces, even when a dicarbonyl is present only one symmetric vibrational mode is observed due to screening of the asymmetric stretch by the electrons of the underlying metal. The use of isotopically labeled CO enables us to demonstrate that this IR signature was indeed due to a dicarbonyl as opposed to monocarbonyl species. This contrasts with Rh dicarbonyl species on

oxide supports which exhibit both antisymmetric and symmetric CO stretching modes. While the RhCu system reported here is the first example of a dicarbonyl being directly observed on a SAA, we speculate that such species may be quite common for other SAAs that bind CO strongly. Indeed, our DFT calculations have identified two other SAA systems where dicarbonyls are predicted to be stable. Understanding the molecular structures associated with IR signatures is important in the characterization of the active sites of high surface area catalysts and may also open up avenues of catalyst design. In particular, it may enable the discovery of SAAs on which two species can bind to the same active site, which is important, for example, in the context of coupling reactions.

ASSOCIATED CONTENT

Supporting information

Detailed information about the experimental and computational setup. Additional data (additional RAIRS data, DFT calculated CO adsorption energy at different sites, comparison of experimental and theoretical acquired vibration frequencies for different species, Bader charge analysis.)

AUTHOR INFORMATION

Corresponding Authors

Julia Schumann - Department of Chemical Engineering, University College London, London WC1E 7JE, UK; Yusuf Hamied Department of Chemistry, University of Cambridge, Cambridge CB2 1EW, UK; Department of Physics and Astronomy, University College London, London WC1E 6BT, UK Email: j.schumann@ucl.ac.uk

Ryan T. Hannagan - Department of Chemistry, Tufts University, Medford, Massachusetts 02155, USA Email: r.t.hannagan@gmail.com

Authors

Yicheng Wang - Department of Chemistry, Tufts University, Medford, Massachusetts 02155, USA

Elizabeth. E. Happel - Department of Chemistry, Tufts University, Medford, Massachusetts 02155, USA

Volkan Cinar - Department of Chemistry, Tufts University, Medford, Massachusetts 02155, USA

Angelos Michaelides - Yusuf Hamied Department of Chemistry, University of Cambridge, Cambridge CB2 1EW, UK; Department of Physics and Astronomy, University College London, London WC1E 6BT, UK

Michail Stamatakis - Department of Chemical Engineering, University College London, London WC1E 7JE, UK

E. Charles H. Sykes - Department of Chemistry, Tufts University, Medford, Massachusetts 02155, USA

Notes

The authors declare no competing financial interests.

Acknowledgements

Y. W., E. E. H., V. C., E. C. H. S., and R. T. H. acknowledge funding from the Division of Chemical Science, Office of Basic Energy Science, CPIMS Program, US Department of Energy, under grant DE-SC 0004738. M. S., and A. M. acknowledge funding from the Leverhulme Trust, grant RPG-2018-209. J. S. thanks the Alexander von Humboldt Foundation, Germany, for support through a Feodor Lynen Fellowship. J. S., A. M., and M. S. thank the UK Materials and Molecular Modelling Hub, which is partially funded by EPSRC (EP/PO20194/1 and EP/T022213/1); the HEC Materials Chemistry Consortium, which is funded by EPSRC (EP/R029431); and the UCL Research Computing Services for computational resources.

Reference

(1) Yates, J. T.; Duncan, T. M.; Worley, S. D.; Vaughan, R. W. Infrared Spectra of Chemisorbed CO on Rh. *J. Chem. Phys.* **1979**, *70* (3), 1219–1224.

(2) Zaera, F. New Advances in the Use of Infrared Absorption Spectroscopy for the Characterization of Heterogeneous Catalytic Reactions. *Chem. Soc. Rev.* **2014**, *43* (22), 7624–7663.

(3) Ding, K.; Gulec, A.; Johnson, A. M.; Schweitzer, N. M.; Stucky, G. D.; Marks, L. D.; Stair, P. C. Identification of Active Sites in CO Oxidation and Water-Gas Shift over Supported Pt Catalysts. *Science* **2015**, *350* (6257), 189–192.

(4) Green, I. X.; Tang, W.; Neurock, M.; Yates, J. T. Spectroscopic Observation of Dual Catalytic Sites during Oxidation of CO on a Au/TiO 2 Catalyst. *Science* **2011**, *333* (6043), 736–739.

(5) Gates, B. C.; Flytzani-Stephanopoulos, M.; DIxon, D. A.; Katz, A. Atomically Dispersed Supported Metal Catalysts: Perspectives and Suggestions for Future Research. *Catal. Sci. Technol.* **2017**, *7* (19), 4259–4275.

(6) DeRita, L.; Dai, S.; Lopez-Zepeda, K.; Pham, N.; Graham, G. W.; Pan, X.; Christopher, P. Catalyst Architecture for Stable Single Atom Dispersion Enables Site-Specific Spectroscopic and Reactivity Measurements of CO Adsorbed to Pt Atoms, Oxidized Pt Clusters, and Metallic Pt Clusters on TiO2. *J. Am. Chem. Soc.* **2017**, *139* (40), 14150–14165.

(7) Qiao, B.; Wang, A.; Yang, X.; Allard, L. F.; Jiang, Z.; Cui, Y.; Liu, J.; Li, J.; Zhang, T. Single-Atom Catalysis of CO Oxidation Using Pt1/FeOx. *Nat. Chem.* **2011**, *3* (8), 634–641.

(8) Sun, G.; Zhao, Z. J.; Mu, R.; Zha, S.; Li, L.; Chen, S.; Zang, K.; Luo, J.; Li, Z.; Purdy, S. C.; Kropf, A. J.; Miller, J. T.; Zeng, L.; Gong, J. Breaking the Scaling Relationship via Thermally Stable Pt/Cu Single Atom Alloys for Catalytic Dehydrogenation. *Nat. Commun.* **2018**, *9* (1).

(9) Hannagan, R. T.; Giannakakis, G.; Réocreux, R.; Schumann, J.; Finzel, J.; Wang, Y.; Michaelides, A.; Deshlahra, P.; Christopher, P.; Flytzani-Stephanopoulos, M.; Stamatakis, M.; Sykes, E. C. H. First-Principles Design of a Single-Atom-Alloy Propane Dehydrogenation Catalyst. *Science* **2021**, *372* (6549), 1444–1447.

(10) Greiner, M. T.; Jones, T. E.; Beeg, S.; Zwiener, L.; Scherzer, M.; Girgsdies, F.; Piccinin, S.; Armbrüster, M.; Knop-Gericke, A.; Schlögl, R. Free-Atom-like d States in Single-Atom Alloy Catalysts. *Nat. Chem.* **2018**, *10* (10), 1008–1015.

(11) Giannakakis, G.; Kress, P.; Duanmu, K.; Ngan, H. T.; Yan, G.; Hoffman, A. S.; Qi, Z.; Trimpalis, A.; Annamalai, L.; Ouyang, M.; Liu, J.; Eagan, N.; Biener, J.; Sokaras, D.; Flytzani-Stephanopoulos, M.; Bare, S. R.; Sautet, P.; Sykes, E. C. H. Mechanistic and Electronic Insights into a Working NiAu Single-Atom Alloy Ethanol Dehydrogenation Catalyst. *J. Am. Chem. Soc.* **2021**.

(12) Marcinkowski, M. D.; Darby, M. T.; Liu, J.; Wimble, J. M.; Lucci, F. R.; Lee, S.; Michaelides, A.; Flytzani-Stephanopoulos, M.; Stamatakis, M.; Sykes, E. C. H. Pt/Cu Single-Atom Alloys as Coke-Resistant Catalysts for Efficient C-H Activation. *Nat. Chem.* **2018**, *10* (3), 325–332.

(13) Lucci, F. R.; Liu, J.; Marcinkowski, M. D.; Yang, M.; Allard, L. F.; Flytzani-Stephanopoulos, M.; Sykes, E. C. H. Selective Hydrogenation of 1,3-Butadiene on Platinum-Copper Alloys at the Single-Atom Limit. *Nat. Commun.* **2015**, *6*, 1–8.

(14) Kyriakou, G.; Boucher, M. B.; Jewell, A. D.; Lewis, E. A.; Lawton, T. J.; Baber, A. E.; Tierney, H. L.; Flytzani-Stephanopoulos, M.; Sykes, E. C. H. Isolated Metal Atom Geometries as a Strategy for Selective Heterogeneous Hydrogenations. *Science* **2012**, *335* (6073), 1209–1212.

(15) Hannagan, R. T.; Giannakakis, G.; Flytzani-Stephanopoulos, M.; Sykes, E. C. H. Single-Atom Alloy Catalysis. *Chem. Rev.* **2020**, *120* (21), 12044–12088.

(16) Jiang, L.; Liu, K.; Hung, S.; Zhou, L.; Qin, R.; Zhang, Q.; Liu, P.; Gu, L.; Chen, H. M.; Fu, G.; Zheng, N. Facet Engineering Accelerates Spillover Hydrogenation on Highly Diluted Metal Nanocatalysts. *Nat. Nanotechnol.* **2020**, *15*, 848–853.

(17) Hannagan, R. T.; Patel, D. A.; Cramer, L. A.; Schilling, A. C.; Ryan, P. T. P.; Larson, A. M.; Çınar, V.; Wang, Y.; Balema, T. A.; Sykes, E. C. H. Combining STM, RAIRS and TPD to Decipher the Dispersion and Interactions Between Active Sites in RhCu Single-Atom Alloys. *ChemCatChem* **2020**, *12* (2), 488–493.

(18) Patel, D. A.; Hannagan, R. T.; Kress, P. L.; Schilling, A. C.; Çlnar, V.; Sykes, E. C. H. Atomic-Scale Surface Structure and CO Tolerance of NiCu Single-Atom Alloys. *J. Phys. Chem. C* **2019**, *123* (46), 28142–28147.

(19) van't Blik, H. F. J.; Huizinga, T.; van Zon, J. B. A. D.; Vis, J. C.; Koningsberger, D. C.; Prins, R. Structure of Rhodium in an Ultradispersed Rh/Al2O3 Catalyst as Studied by EXAFS and Other Techniques. *J. Am. Chem. Soc.* **1985**, *107* (11), 3139–3147.

(20) Goellner, J. F.; Gates, B. C.; Vayssilov, G. N.; Rösch, N. Structure and Bonding of a Site-Isolated Transition Metal Complex: Rhodium Dicarbonyl in Highly Dealuminated Zeolite Y. *J. Am. Chem. Soc.* **2000**, *122* (33), 8056–8066.

(21) Han, B.; Guo, Y.; Huang, Y.; Xi, W.; Xu, J.; Luo, J.; Qi, H.; Ren, Y.; Liu, X.; Qiao, B.; Zhang, T. Strong Metal–Support Interactions between Pt Single Atoms and TiO2. *Angew. Chemie - Int. Ed.* **2020**, *59* (29), 11824–11829.

(22) Cheng, M. J.; Clark, E. L.; Pham, H. H.; Bell, A. T.; Head-Gordon, M. Quantum Mechanical Screening of Single-Atom Bimetallic Alloys for the Selective Reduction of CO2 to C1 Hydrocarbons. *ACS Catal.* **2016**, *6* (11), 7769–7777.

(23) Kwon, Y.; Kim, T. Y.; Kwon, G.; Yi, J.; Lee, H. Selective Activation of Methane on Single-Atom Catalyst of Rhodium Dispersed on Zirconia for Direct Conversion. *J. Am. Chem. Soc.* **2017**, *139* (48), 17694–17699.

(24) Zakem, G.; Ro, I.; Finzel, J.; Christopher, P. Support Functionalization as an Approach for Modifying Activation Entropies of Catalytic Reactions on Atomically Dispersed Metal Sites. *J. Catal.* **2021**, *404*, 883–896.

(25) Matsubu, J. C.; Yang, V. N.; Christopher, P. Isolated Metal Active Site Concentration and Stability Control Catalytic CO2 Reduction Selectivity. *J. Am. Chem. Soc.* **2015**, *137* (8), 3076–3084.

(26) Cavanagh, R. R.; Yates, J. T. Site Distribution Studies of Rh Supported on Al2O3 - An Infrared Study of Chemisorbed CO. *J. Chem. Phys.* **1981**, *74* (7), 4150–4155.

(27) Yates, J. T.; Duncan, T. M.; Vaughan, R. W. Infrared Spectroscopic Study of Activated Surface Processes: CO Chemisorption on Supported Rh. *J. Chem. Phys.* **1979**, *71* (10), 3908–3915.

(28) Yang, D.; Xu, P.; Browning, N. D.; Gates, B. C. Tracking Rh Atoms in Zeolite HY: First Steps of Metal Cluster Formation and Influence of Metal Nuclearity on Catalysis of Ethylene Hydrogenation and Ethylene Dimerization. *J. Phys. Chem. Lett.* **2016**, *7* (13), 2537–2543.

(29) Wang, Y.; Papanikolaou, K. G.; Hannagan, R. T.; Patel, D. A.; Balema, T. A.; Cramer, L. A.; Kress, P. L.; Stamatakis, M.; Sykes, E. C. H. Surface Facet Dependence of Competing Alloying Mechanisms. *J. Chem. Phys.* **2020**, *153* (24).

(30) Darby, M. T.; Sykes, E. C. H.; Michaelides, A.; Stamatakis, M. Carbon Monoxide Poisoning Resistance and Structural Stability of Single Atom Alloys. *Top. Catal.* **2018**, *61* (5–6), 428–438.

(31) Papanikolaou, K. G.; Darby, M. T.; Stamatakis, M. CO-Induced Aggregation and Segregation of Highly Dilute Alloys: A Density Functional Theory Study. *J. Phys. Chem. C* **2019**, *123* (14), 9128–9138.

(32) Roiaz, M.; Falivene, L.; Rameshan, C.; Cavallo, L.; Kozlov, S. M.; Rupprechter, G. Roughening of Copper (100) at Elevated CO Pressure: Cu Adatom and Cluster Formation Enable CO Dissociation. *J. Phys. Chem. C* **2019**, *123* (13), 8112–8121.

(33) Zhong, J. Q.; Shaikhutdinov, S.; Roldan Cuenya, B. Structural Evolution of Ga-Cu Model Catalysts for CO2 Hydrogenation Reactions. *J. Phys. Chem. C* **2021**, *125* (2), 1361–1367.

(34) Marcinkowski, M. D.; Murphy, C. J.; Liriano, M. L.; Wasio, N. A.; Lucci, F. R.; Sykes, E. C. H. Microscopic View of the Active Sites for Selective Dehydrogenation of Formic Acid on Cu(111). *ACS Catal.* **2015**, *5* (12), 7371–7378.

(35) Mason, S. E.; Grinberg, I.; Rappe, A. M. Adsorbate-Adsorbate Interactions and

Chemisorption at Different Coverages Studied by Accurate Ab Initio Calculations: CO on Transition Metal Surfaces. *J. Phys. Chem. B* **2006**, *110* (8), 3816–3822.

(36) Lausche, A. C.; Medford, A. J.; Khan, T. S.; Xu, Y.; Bligaard, T.; Abild-Pedersen, F.; Nørskov, J. K.; Studt, F. On the Effect of Coverage-Dependent Adsorbate-Adsorbate Interactions for CO Methanation on Transition Metal Surfaces. *J. Catal.* **2013**, *307*, 275–282.

(37) Muir, M.; Trenary, M. Adsorption of CO to Characterize the Structure of a Pd/Ag(111) Single-Atom Alloy Surface. *J. Phys. Chem. C* **2020**, *124* (27), 14722–14729.

(38) Therrien, A. J.; Hensley, A. J. R.; Marcinkowski, M. D.; Zhang, R.; Lucci, F. R.; Coughlin, B.; Schilling, A. C.; McEwen, J. S.; Sykes, E. C. H. An Atomic-Scale View of Single-Site Pt Catalysis for Low-Temperature CO Oxidation. *Nat. Catal.* **2018**, *1* (3), 192–198.

(39) Frank, M.; Kühnemuth, R.; Bäumer, M.; Freund, H. J. Vibrational Spectroscopy of CO Adsorbed on Supported Ultra-Small Transition Metal Particles and Single Metal Atoms. *Surf. Sci.* **2000**, *454* (1), 968–973.

(40) Lee, H. J.; Ho, W. Single-Bond Formation and Characterization with a Scanning Tunneling Microscope. *Science* **1999**, *286* (5445), 1719–1722.

(41) Liu, J.; Lucci, F. R.; Yang, M.; Lee, S.; Marcinkowski, M. D.; Therrien, A. J.; Williams, C. T.; Sykes, E. C. H.; Flytzani-Stephanopoulos, M. Tackling CO Poisoning with Single-Atom Alloy Catalysts. *J. Am. Chem. Soc.* **2016**, *138* (20), 6396–6399.